Supporting Information:

Quantifying Nanosheet Graphene Oxide using Electrospray Differential Mobility Analysis

Jui-Ting Tai,[1] Yen-Chih Lai,[1,2] Chien-Ho Yang,[1] Hsin-Chia Ho,[2] Hsiao-Fang Wang,[1] Rong-Ming Ho,[1] De-Hao Tsai[1,]*

1: Department of Chemical Engineering, National Tsing Hua University, Hsinchu, Taiwan, ROC

2: Center for Measurement Standards, Industrial Technology Research Institute, Hsinchu, Taiwan, ROC

[*]Corresponding Author: Email: dhtsai@mx.nthu.edu.tw; Phone: 886-3-5169316; Fax: 886-3-5715408

1. Instrumentation Parameters of ES-DMA

The following are the parameters used to calculate $d_{p,m}$ by the Eq. 1 of the main text:[1,2]

$$K_1 = \frac{2neL}{3\ln(r_2 / r_1)} \qquad \text{(S1)}$$

n = number of elementary charges on the particle (=1 for singly charged particles)

e = elementary charge (1.6 x 10^{-19} Coulomb)

C_c = Cunningham slip correction =1+Kn[α+β exp(-γ/Kn)]

α = 1.142, β = 0.558, γ = 0.999

Kn = Knudsen Number = $2\lambda/d_{p,m}$

λ: mean free path of air (=66 nm)

μ = gas viscosity

r_2 = outer radius of annular space= 1.905 cm

r_1 = inner radius of annular space= 0.937 cm

L = length between exit slit and polydisperse aerosol inlet = 4.987 cm

2. Additional TEM images

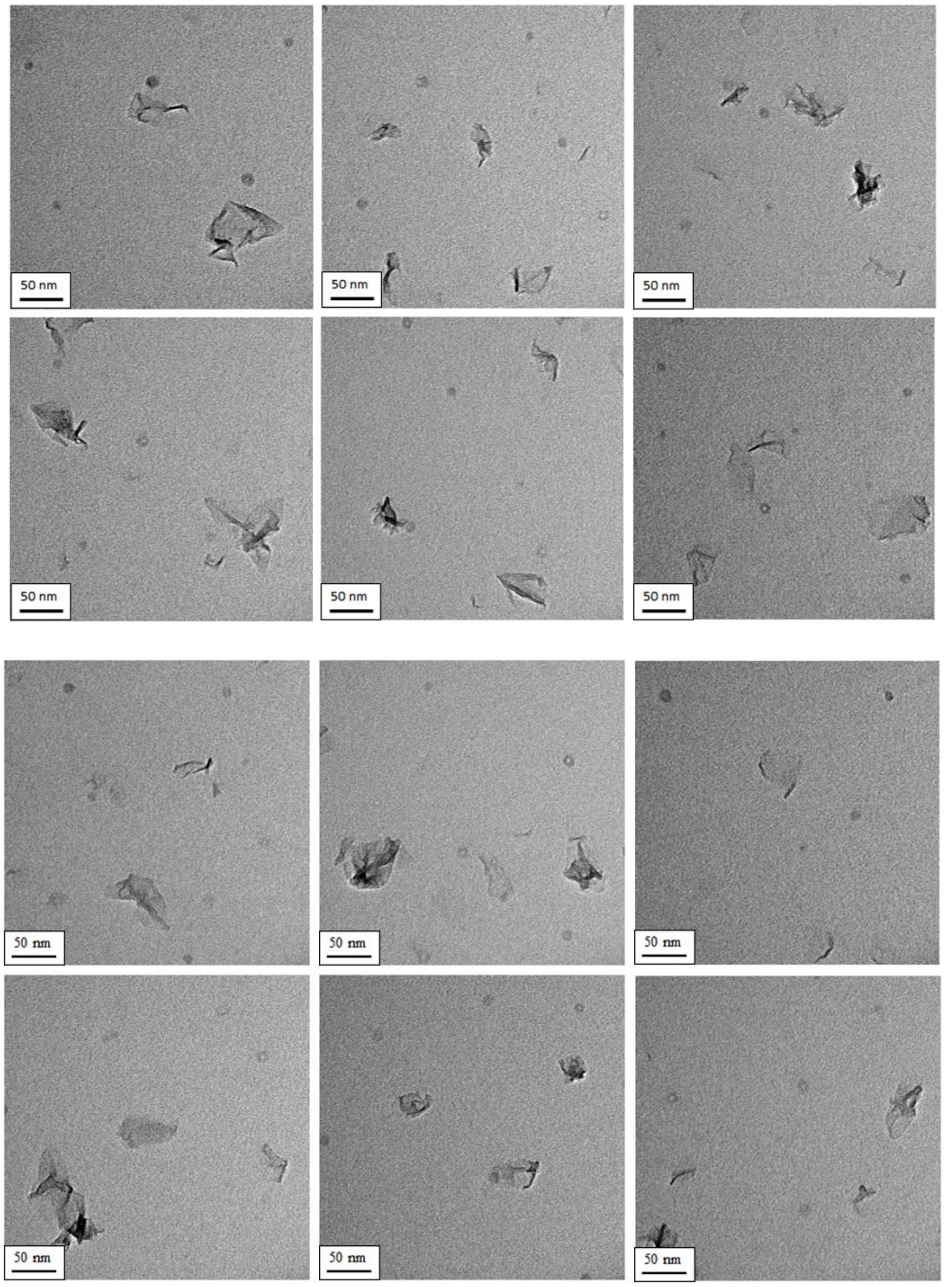

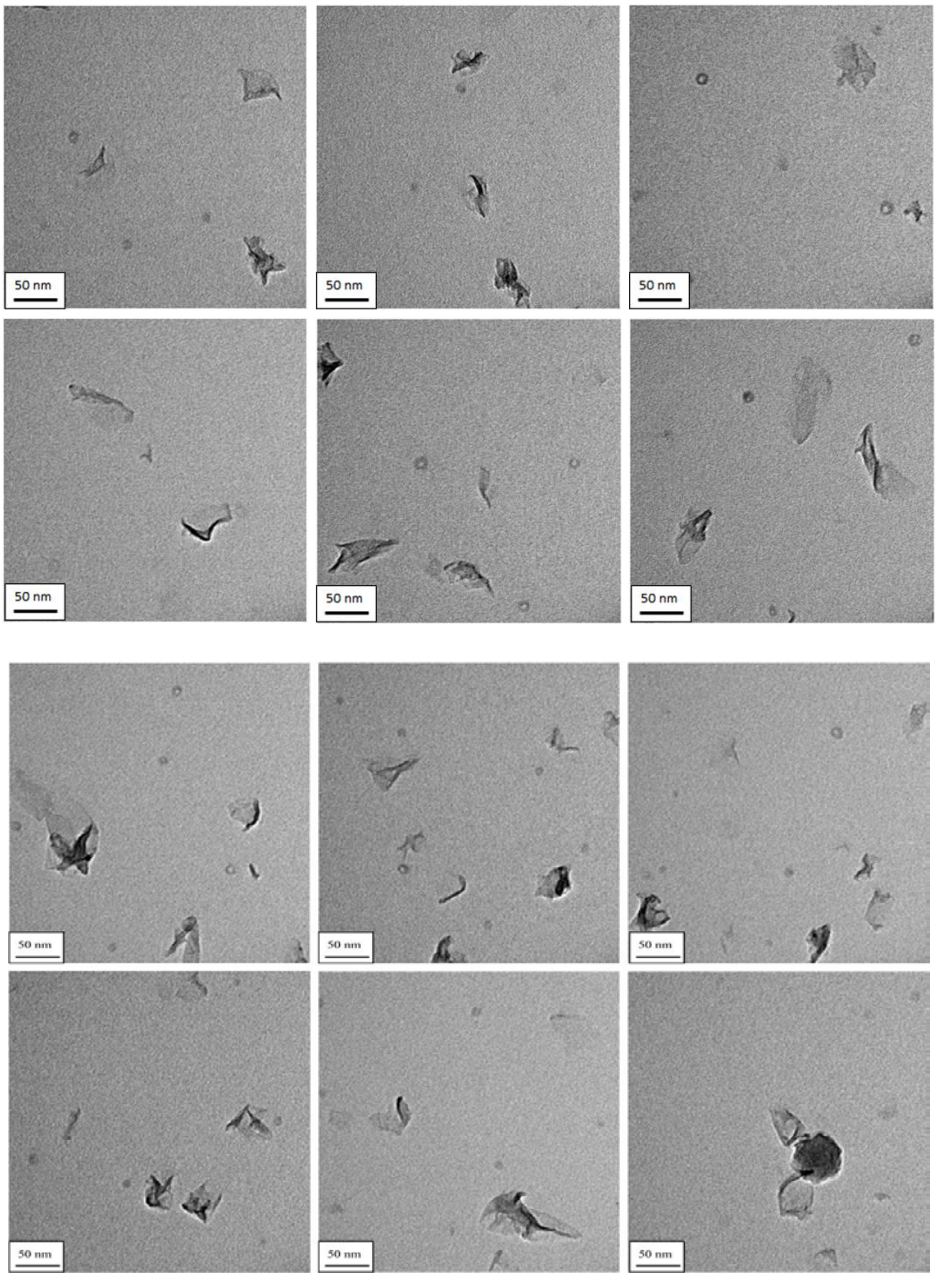

Figure S1. Additional TEM images of the electrosprayed N-GOs without size classification. The scale bars were 50 nm for all images.

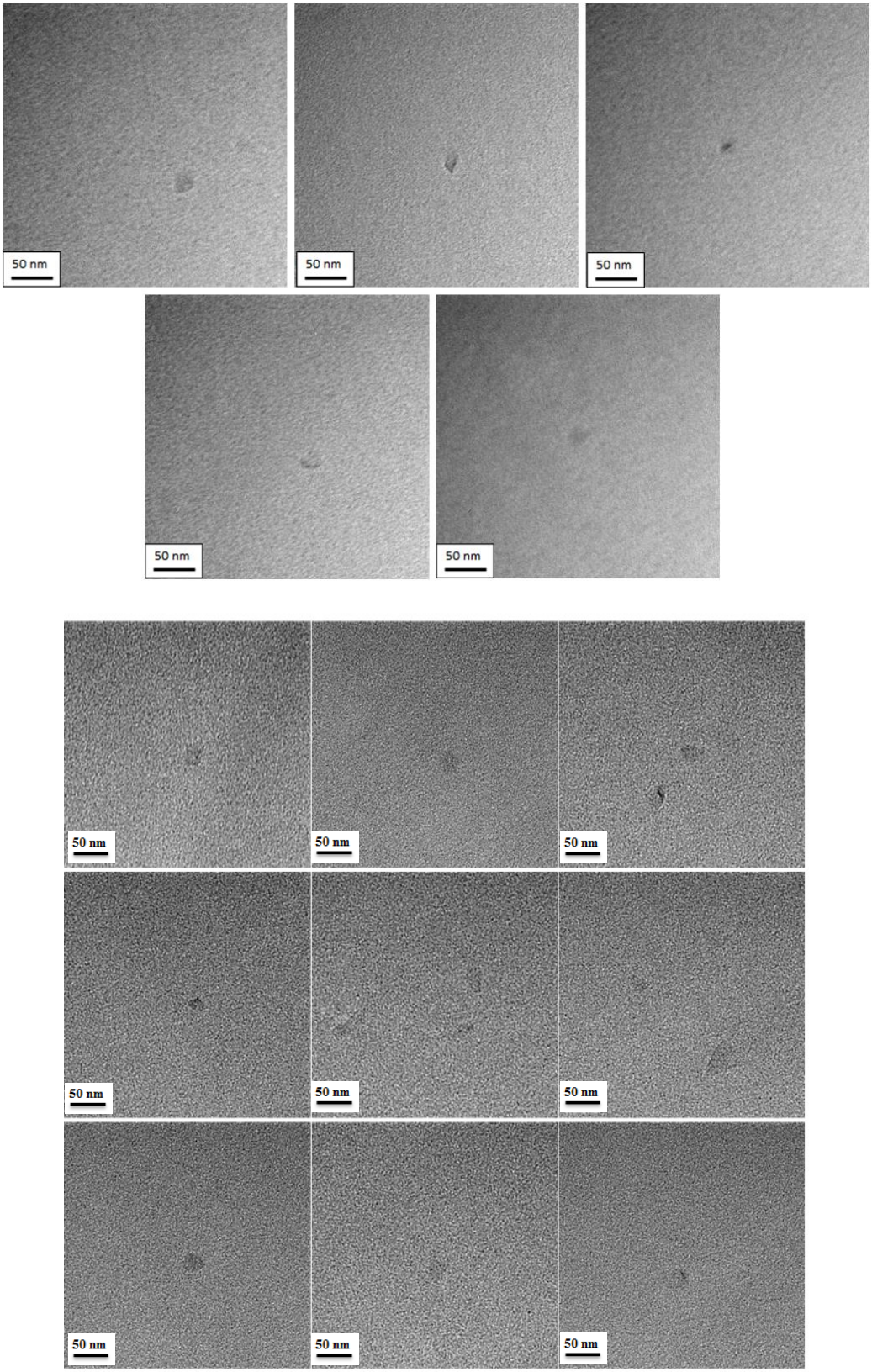

Figure S2-1. Additional TEM images of the electrosprayed N-GOs. Size-selected at $d_{p,m}$=20 nm. The scale bars were 50 nm for all images.

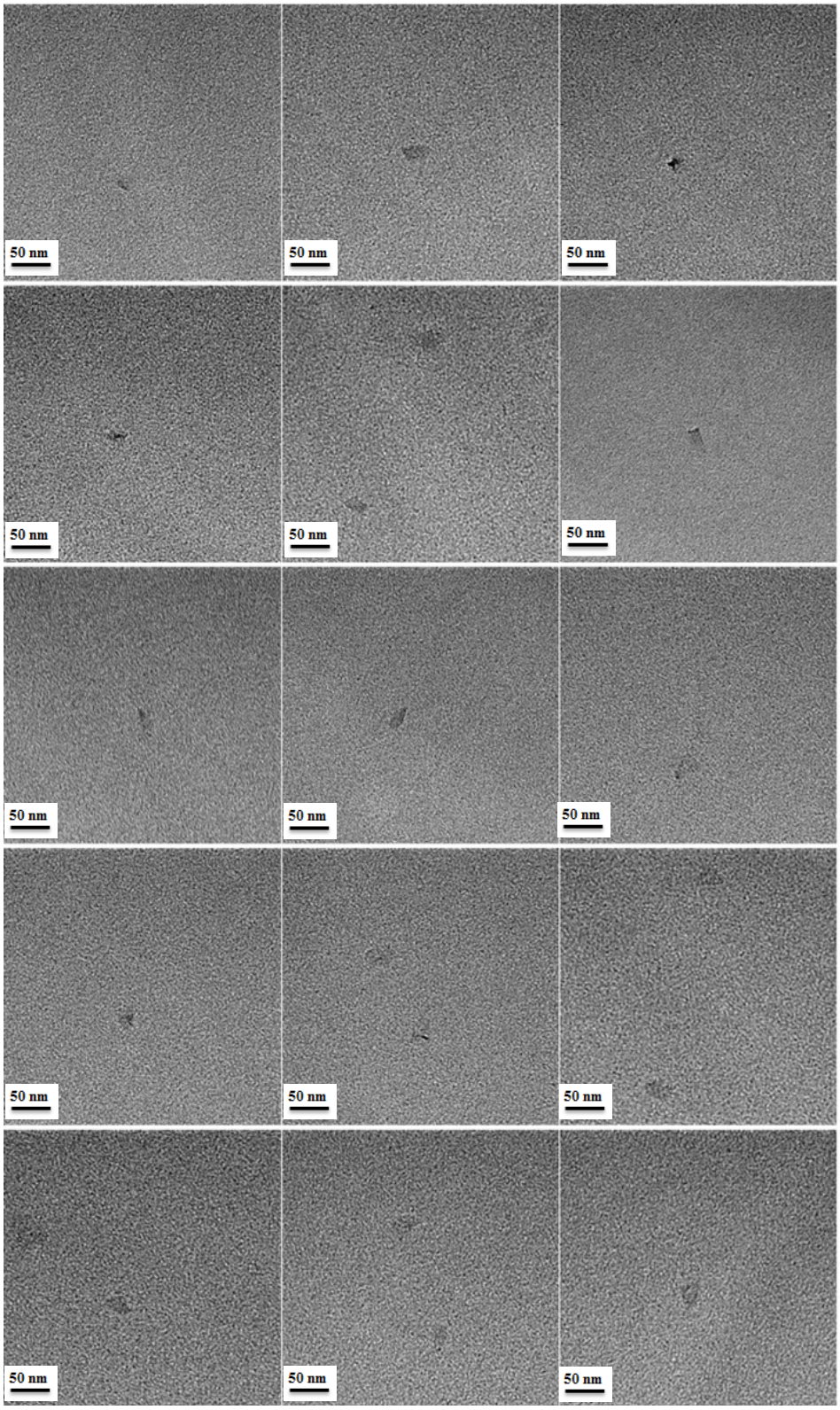

Figure S2-2. Additional TEM images of the electrosprayed N-GOs. Size-selected at $d_{p,m}$=20 nm. The scale bars were 50 nm for all images.

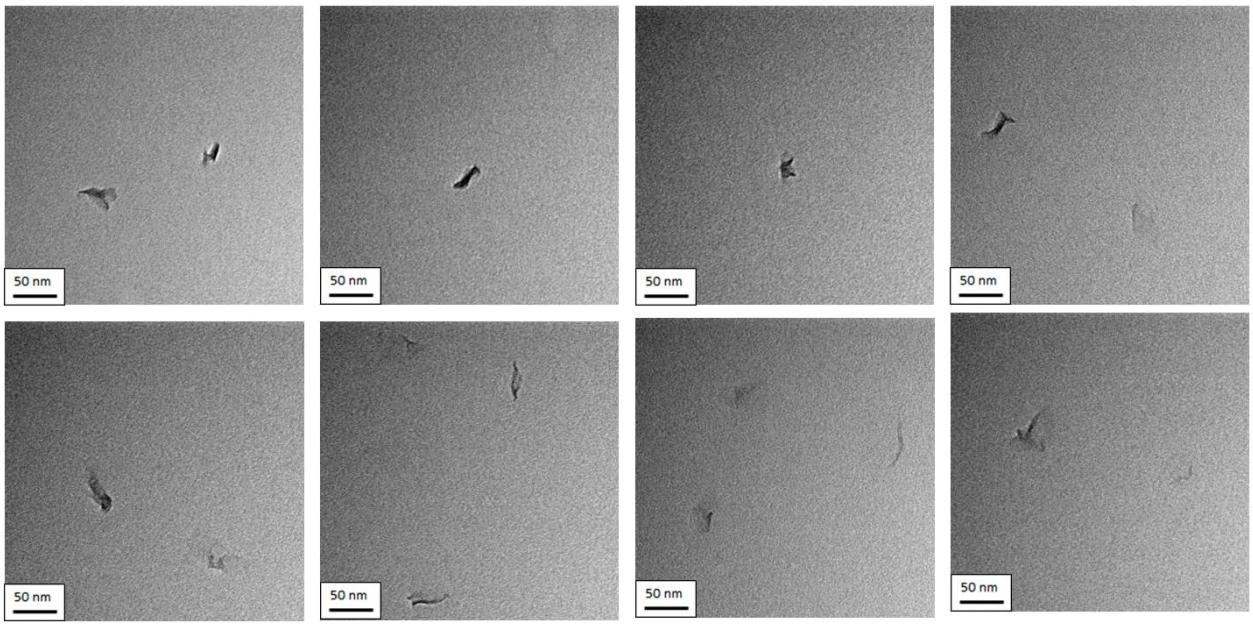

Figure S3 -1. Additional TEM images of the electrosprayed N-GOs. Size-selected at $d_{p,m}$=33 nm. The scale bars were 50 nm for all images.

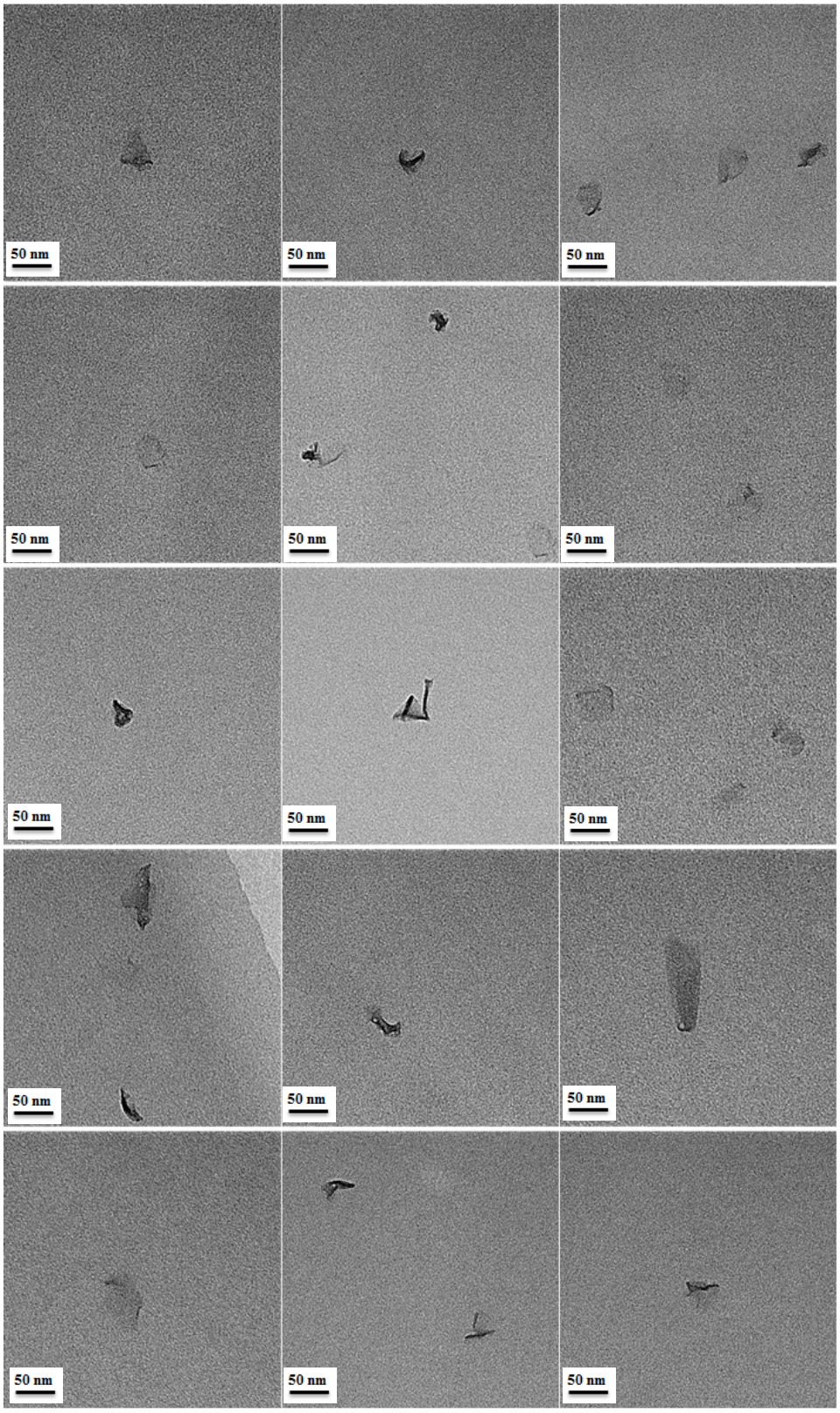

Figure S3-2. Additional TEM images of the electrosprayed N-GOs. Size-selected at $d_{p,m}$=33 nm. The scale bars were 50 nm for all images.

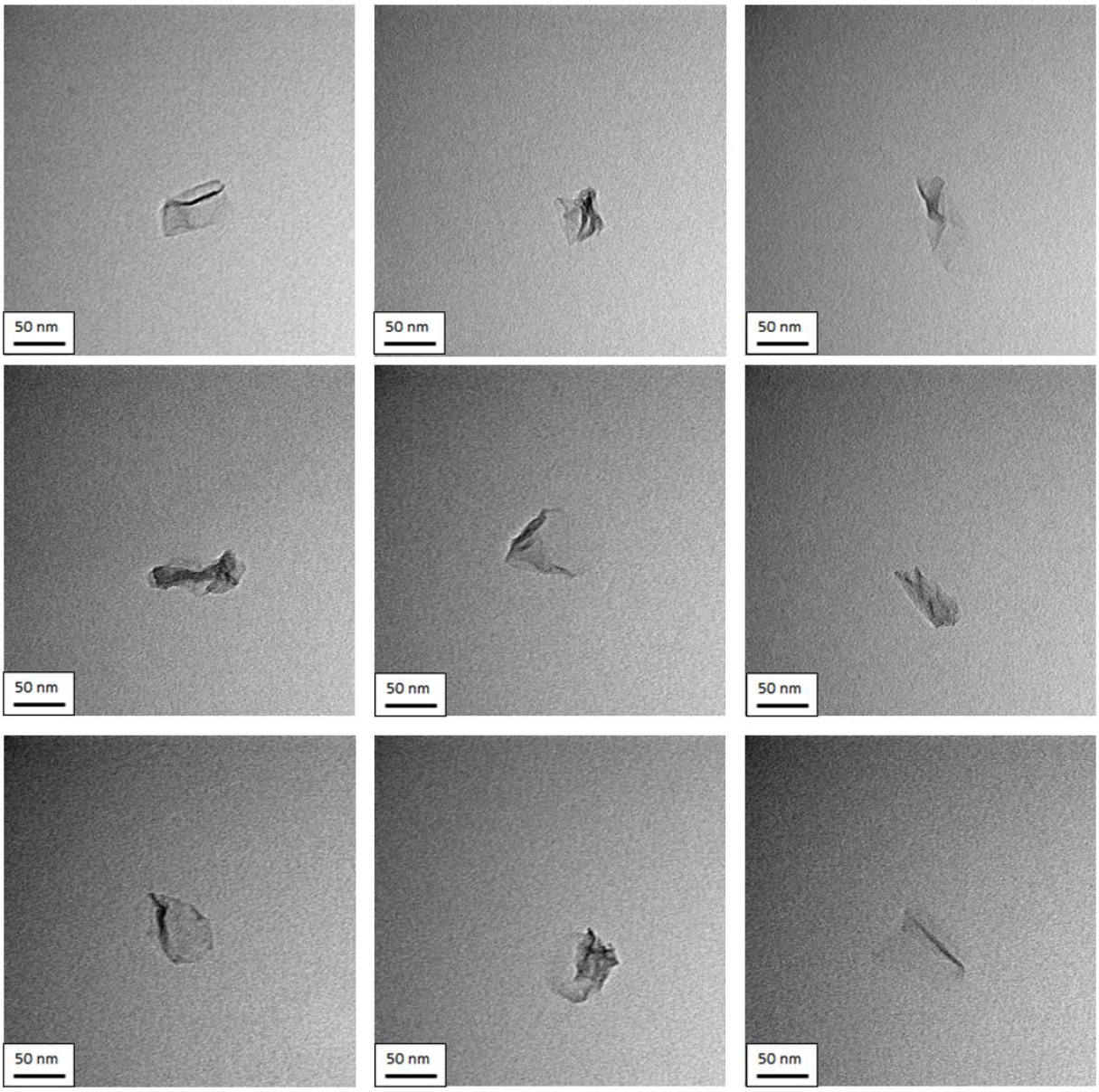

Figure S4-1. Additional TEM images of the electrosprayed N-GOs. Size-selected N-GOs at $d_{p,m}$=57 nm. The scale bars were 50 nm for all images.

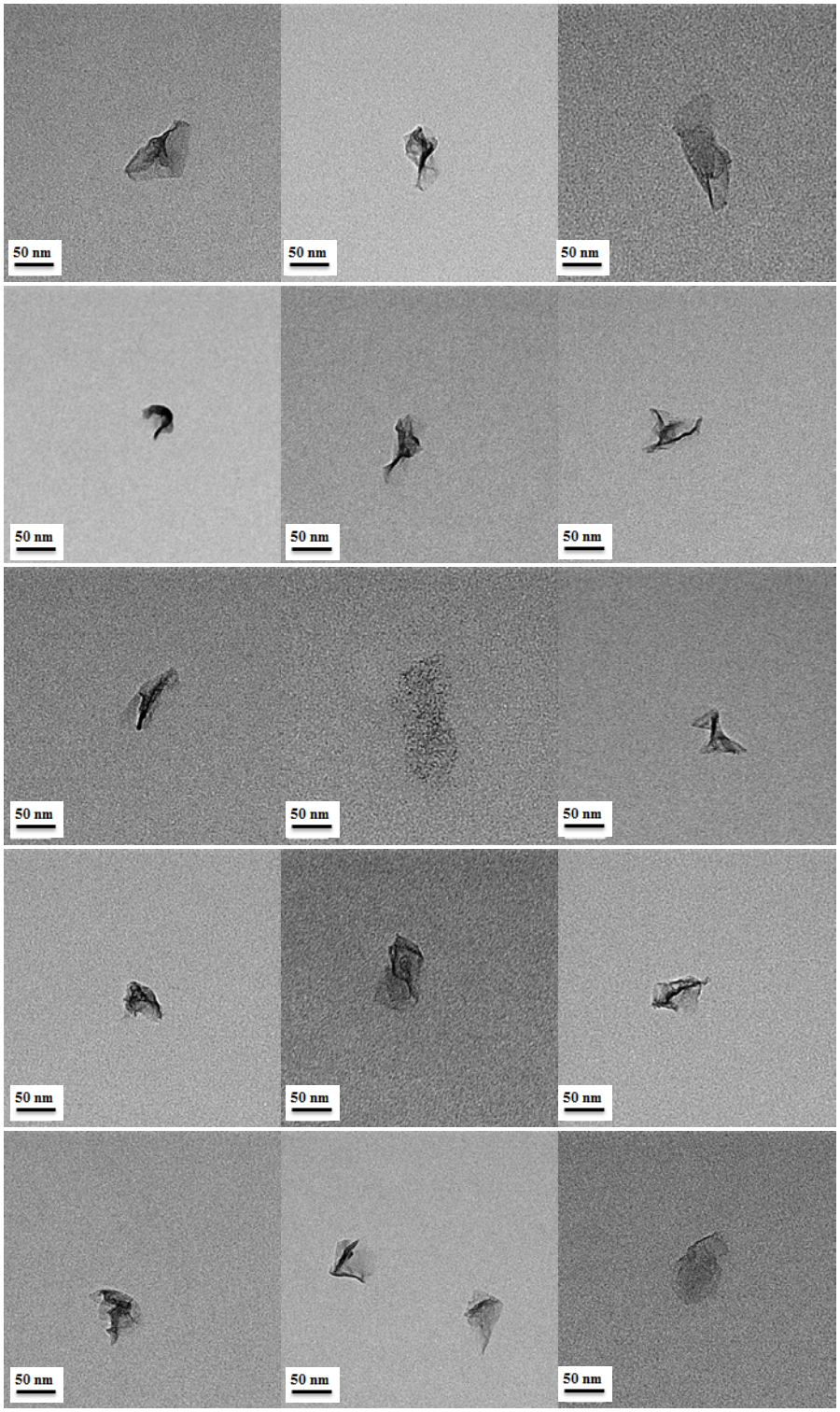

Figure S4-2. Additional TEM images of the electrosprayed N-GOs. Size-selected N-GOs at $d_{p,m}$=57 nm. The scale bars were 50 nm for all images.

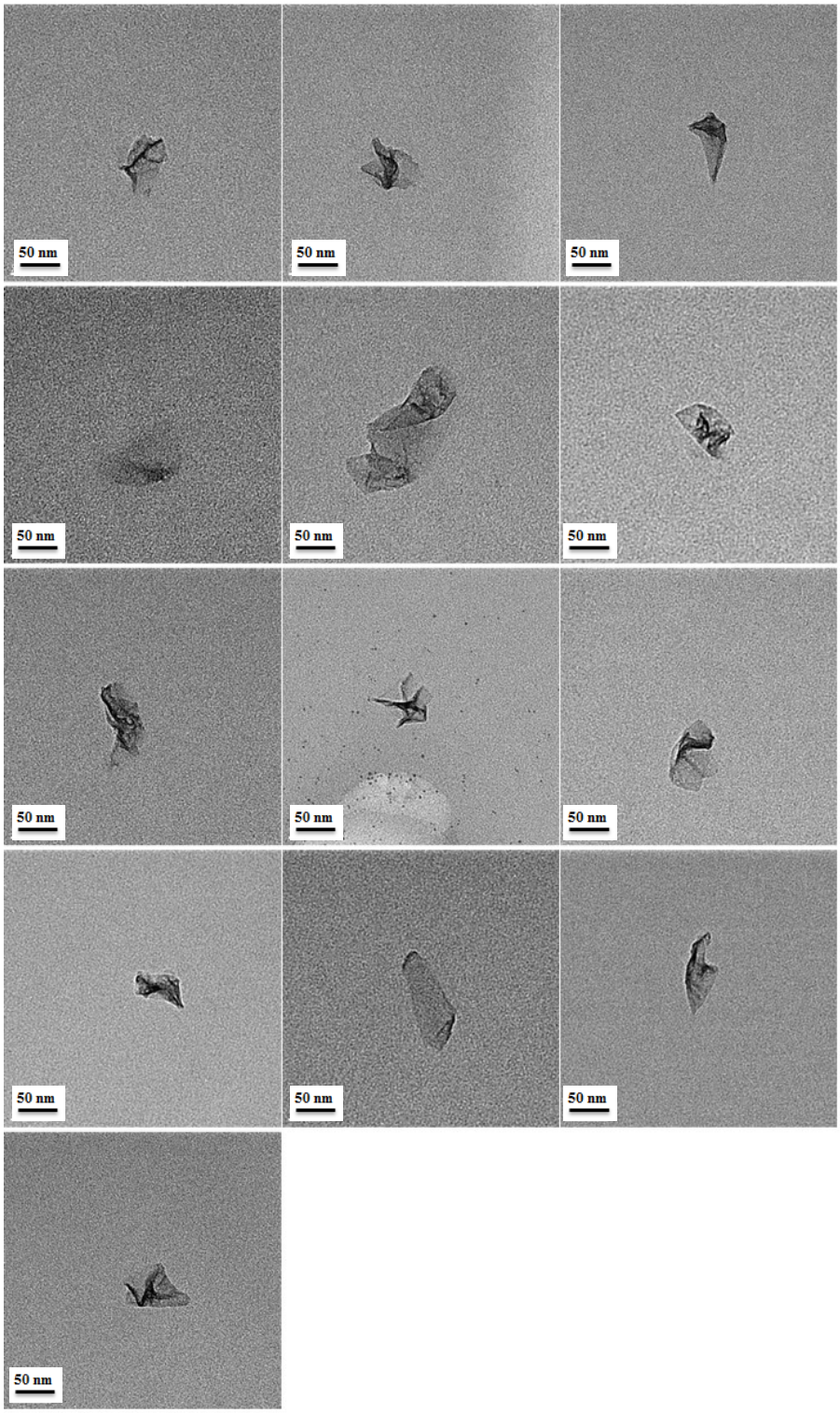

Figure S4-3. Additional TEM images of the electrosprayed N-GOs. Size-selected N-GOs at $d_{p,m}$=57 nm. The scale bars were 50 nm for all images.

3. Determination of the Projected Area of N-GOs (A_p) measured by TEM

Figure S5 demonstrates the method to calculate the A_p based on the TEM image. From the scale bars of the TEM images, we calculated the area of a grid, A_{grid}. Then the number of grids occupied by the projected N-GOs (N_{grid}) were counted for the determination of A_p ($=N_{grid}\times A_{grid}$). The lateral resolution of the grid was ≈2 nm.

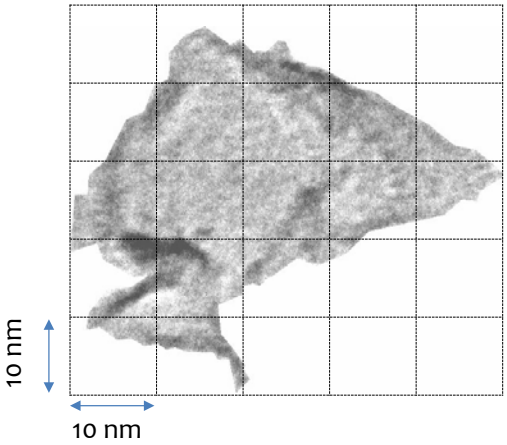

Figure S5. Determination of the projected area of a N-GO (A_p) using a TEM image.

4. Derivation of $N_{p,g}$ and $N_{p,g,PS}$

By integrating the peaks for N-GOs in the size distribution obtained by ES-DMA, $N_{p,g}$, and the $N_{p,g,PS}$ were determined using Eq. S2:[3-7]

$$N_{p,g} = \int_{d_{p,m,min}}^{d_{p,m,max}} \frac{dN_p}{dd_p} ddp \qquad \text{(S2)}$$

where dN_p/dd_p is the number intensity of N-GOs in the gas phase at a specific $d_{p,m,}$ after considering the charge efficiency of a singly charged N-GO (i.e., size-dependent).[1,2,6] $d_{p,m,max}$ and $d_{p,m,min}$ were the maxima and minima mobility diameters bounding a peak corresponding to N-GOs, respectively. dd_p was calculated based on the ratio of aerosol flow rate to sheath flow rate, a key component to determine the transfer function of DMA. For simplicity, we use $dd_p=0.2\times d_{p,m}$. A corrected value for

the mobility size of N-GO was obtained by further taking into account the contribution from the salt residues encrusted on N-GOs with the expression of Eq. S3,[8,9]

$$d_{p,m,corrected} = \sqrt[3]{d_{p,m}^{\ 3} - d_s^{\ 3}} \qquad \text{(S3)}$$

where $d_{p,m}$ and d_s are mobility diameter of the N-GO encrusted with dried solvent remnant and the S-NP, respectively.

In addition, we consider the possible effect of droplet-induced aggregation discussed in the previous works.[6,7,10] Due to the relative low particle concentration and small droplet size (≈150 nm), the probability to have one particle in a droplet is only 1% at C_p=0.01. Hence the effect of multiple N-GOs per droplet was negligible at low C_p. It was likely that the probability could be increased when C_p was 0.1, but we did not observe any significant change in the distribution and also the average $d_{p.m}$ in our results (see the Fig. 3a of the main text).

5. Additional PSDs Measured by ES-DMA

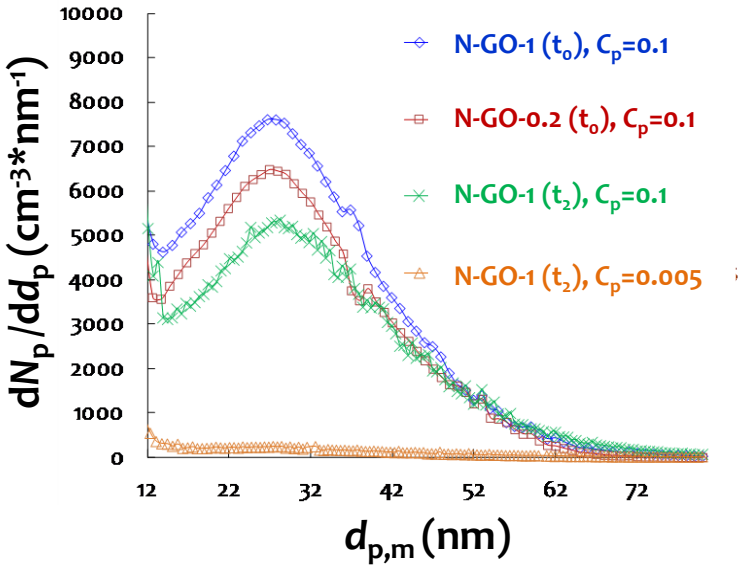

Figure S6. Mobility size distributions of N-GOs after considering corrections of the charge ratio, the encrusted layer of dried solvent remnant, and the transfer function of DMA.

6. Determination of the Density of N-GOs

The reported values of the density of N-GO (ρ_{GO}) are varied from 0.03 g/cm^3 to 2.2 g/cm^3 in the literatures.[11-15] The variations could be due to the measured results by different types of instruments or methods, and the differences in the theoretical calculations assuming a compact film or a bulk GO. We choose to use ρ_{GO}=0.3 g/cm^3 reported by Schniepp et. al.[11] due to a better fitting to the lateral size distribution measured by TEM.

As stated in the main text, we need to consider a range of density to the fitted L_t-distribution. Fig. S7 demonstrates the results of the L_t-distributions over various δ_{GO} by choosing ρ_{GO} =1.8 g/cm^3. As seen, even δ_{GO} is as small as 0.4 nm (one layer of graphene), the calculated L_t is still shown to be less than the L_t measured by TEM. Also, from the literature reported values, the minimum δ_{GO} should be at least ≈(0.7-0.8) nm for a monolayer GO. Hence we choose to use 0.3 g/cm^3 since the results of L_t provide a better fit to the TEM analysis and also the δ_{GO} used is close to the reported value in literatures.

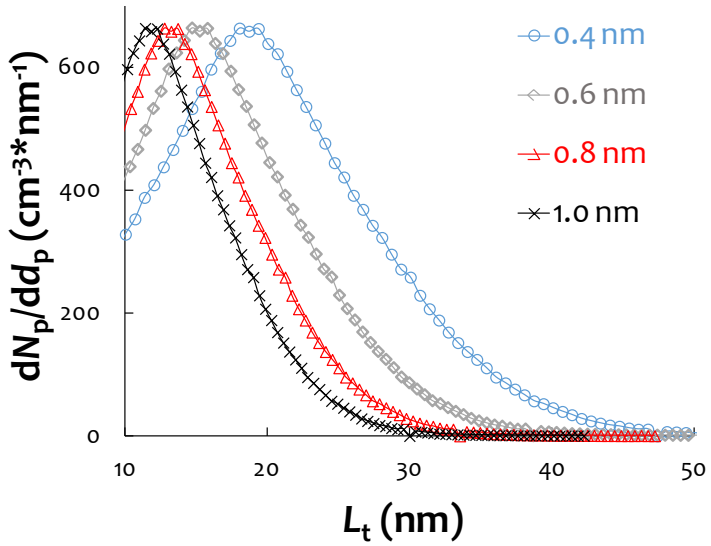

Figure S7. Lateral size distributions of N-GOs derived from the DMA results of Fig. 2a of the main text, assuming ρ_{GO} =1.8 g/cm^3. Sample: N-GO-1 (t0) at C_p=0.01. Four different δ_{GO} values ranging from 0.4 nm to 1.0 nm are chosen in the calculation.

Figure S8 shows the effect of ρ_{GO} on the L_t-distributions. By increasing ρ_{GO}, we observed that L_t was decreased under two different δ_{GO} values. For δ_{GO}= 0.8 nm (Fig. S8a), we could see a better fit was shown at ρ_{GO} =0.3 g/cm^3. While increasing the δ_{GO} to 2.0 nm, we observed the best fitted value of ρ_{GO} was decreased to 0.1 g/cm^3, proportional to 1/δ_{GO}. Based on the electron contrast shown in TEM images (Fig. S2) and the SPM results measured on a large GO sheet,[16,17] we assume N-GO is monolayer. However, a limitation to this current method is that the calculated results may not be able to distinguish the accuracy ranging from ρ_{GO} =0.22 g/cm^3 to ρ_{GO}=0.34 g/cm^3 by assuming δ_{GO} ranging from 0.7 nm to 1.1 nm, respectively (i.e., resulting in identical lateral size distributions). Future work seeks to improve the accuracy in the determination of ρ_{GO}.

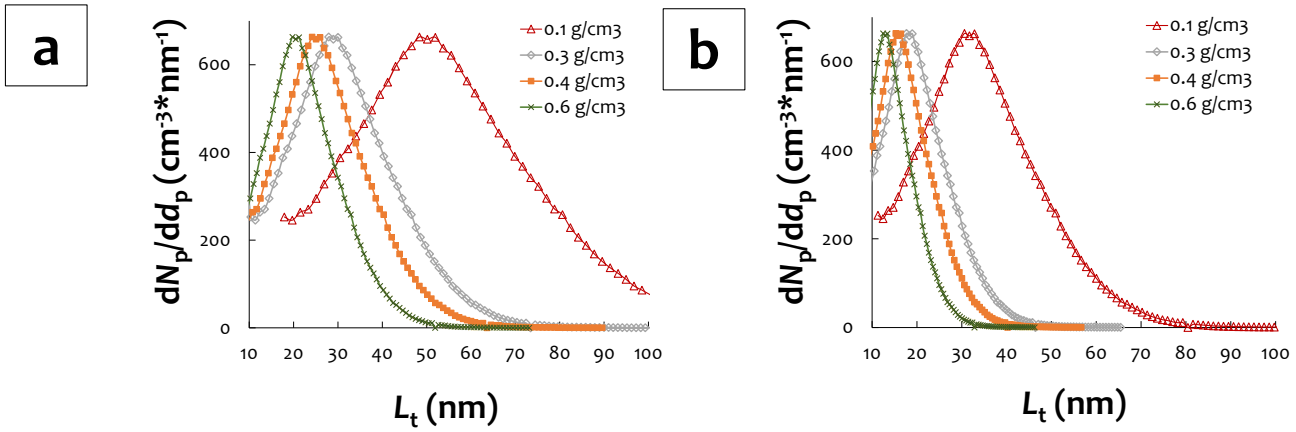

Figure S8. Lateral size distributions of N-GOs derived from the DMA results of Fig. 2a of the main text. Sample: N-GO-1 (t0) at C_p=0.01. Four different ρ_{GO} values ranging from 0.1 g/cm^3 nm to 0.6 g/cm^3 are chosen in the calculation. (a) δ_{GO} =0.8 nm. (b) δ_{GO} =2 nm.

7. Determination of Charge Efficiency and Charge Distribution

Aerosol particles acquire charges by collision with ions in a chamber containing a Po 210 source (TSI Inc.). Because of their random thermal motion, those aerosol particles will lose their initial charges slowly as the charged particles attract oppositely charged ions, eventually leading to

an equilibrium charge state called the Boltzmann equilibrium charge distribution. For equal concentrations of positive and negative ions, the fraction of particles f_n of a given size (d_p) having n positive elementary units of charge can be calculated using Eq. S4:[1,2]

$$f_n = \frac{\exp(\frac{K_E n^2 e^2}{d_p kT})}{\Sigma_{n=-\infty}^{\infty} \exp(\frac{K_E n^2 e^2}{d_p kT})} \quad . \qquad \text{(S4)}$$

Here K_E is a constant of proportionality (=9.0*10^9 N*m^2*C^{-2}). By calculation, f_n≈10 % for 30 nm-sized N-GOs.

Experimentally, we choose to use spherical-like, nominally 30-nm gold nanoparticle standard reference materials (30-AuNP. National Institute of Standards and Technology, U.S.A)[18] to measure charge state at the range of mobility size we study. The electrical mobility (Z_e) of the measured aerosol particles can be expressed as a function of the number of elementary charges on the particles (n):[1]

$$Z_e = \frac{neC_c}{3\pi\mu d_{p,m}} \qquad \text{(S5)}$$

Where μ is the viscosity of air, and C_c is the Cunningham slip correction, which can be calculated using Eq. S6:[1,2]

$$C_c = 1 + K_n[\alpha + \beta \exp(-\gamma/K_n)] \qquad \text{(S6).}$$

Here α= 1.142, β = 0.558, γ = 0.999. $K_n = 2\lambda/d_{p,m}$, where λ is the gas mean free path (≈66 nm for air at room temperature). Figure S9a shows the mobility distribution of 30-nm AuNP. As seen, Z_e of 30-nm AuNP was peaked at (2.2-2.3)*10^{-7} m^2*$volt^{-1}$*s^{-1}. Based on the design of electrostatic classifier, polarity of electric field (negative), and carrier gas flow rate, the measured Z_e can be expressed as

$$Z_e = Q_{sh}/(2\pi V_{DMA} L)*\ln(r_2/r_1) \qquad \text{(S7),}$$

where Q_{sh} is the flow rate of sheath air in DMA, L is the length between exit slit and polydisperse aerosol inlet, and V_{DMA} is the applied DC voltage to the DMA. r_2 and r_1 are outer and inner radius of DMA, respectively (see Section S1).[2] Combing Eq. S6 and Eq. S7 we obtain Eq. S8 and then convert Fig. S9a into Fig. S9b:

$$n = 3\,\mu\, d_{p,m}{}^{*}Q_{sh}/(2\pi e V_{DMA} L C_c)^{*}\ln(r_2/r_1) \qquad \text{(S8)}.$$

From Fig. S9b we can see the charge distribution of the aerosol particles (30-nm AuNP) are mainly singly charged (+1). Results confirm that the dominant charge state in the mobility size range we considered is +1 after electrospray ionization and charge neutralization in gas phase.

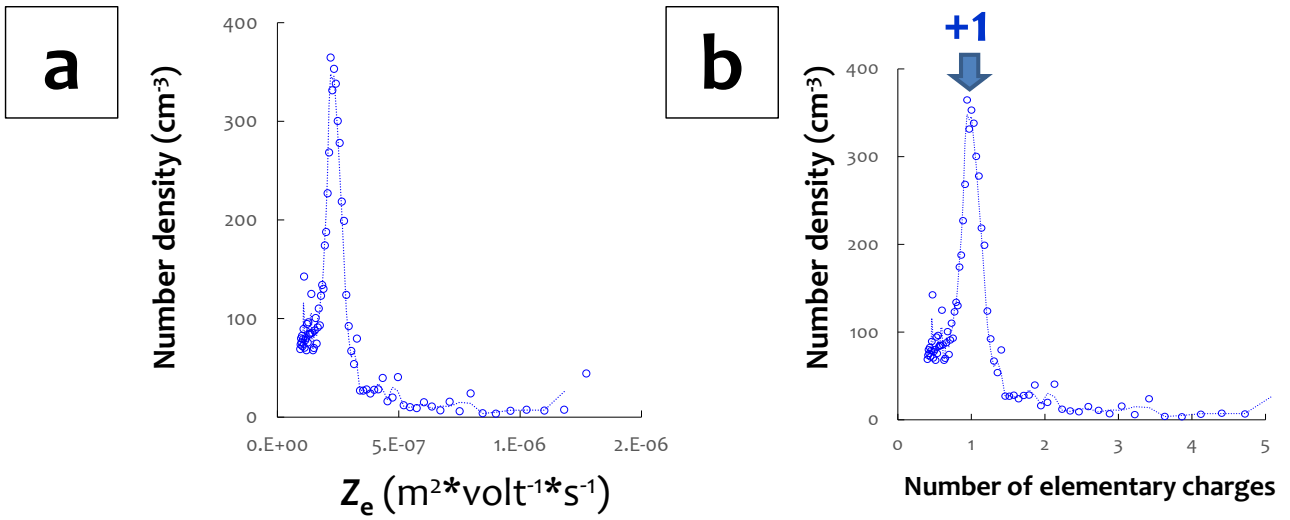

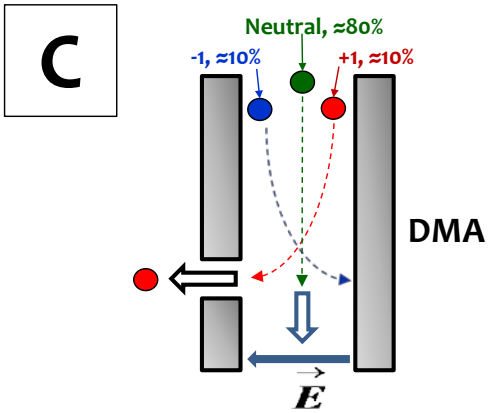

Figure S9. Analysis of the charge state of aerosolized particles. (a) Mobility distribution of 30-nm AuNP. (b) Analysis of number of elementary charges per 30-nm AuNP. (c) Cartoon depiction of particle trajectories in DMA.

Figure S9c shows a cartoon depiction to describe the trajectories of aerosol particles ($d_{p,m}$≈30 nm) in DMA. Neutral particles cannot be selected by DMA due to the lack of influence by the applied electric field (i.e., carried out of the DMA by the sheath air). Since we use an electric field with negative polarity, the particles entering the slit of center rod are +1, where the particles with negative charges shall be deposited on the outer annular space of DMA.[1]

Experimentally we choose to use silica nanoparticles (LUDOX® TM-40 colloidal silica, Sigma-Aldrich, MO, U.S.A) to see whether the measured mobility coefficient distributions would be insensitive to pH (i.e., different charge states) or not. The reason of using colloidal silica is the high colloidal stability over a broad range of pH (i.e., without inducing unwanted conformation changes). Figure S10a shows the mobility size distributions of SiO_2 nanoparticles under three different pH conditions: pH 2, pH 7, and pH 9, having corresponding zeta potentials of ≈0 mV, ≈-39 mV, and ≈-46 mV, respectively. As seen, the mobility size distributions of SiO_2 nanoparticles were shown to be almost identical, even though a significant difference in the surface charges in solution phase (i.e., zeta potentials were ranging from 0 mV to -46 mV). Note that the zeta potentials were measured using a Malvern Nano Zetasizer equipped with disposable folded capillary cells.[3]

We also compare the mobility size distributions of N-GO at two different pH conditions (i.e., colloidally stable with different zeta potentials: ≈-60 mV at pH 4.5 and -73 mV at pH 9.0). Figure 10b shows the mobility size distributions of N-GOs at pH 4.5 and at pH 9.0. Results show that the mobility diameters measured under these two pH values were quite close: $d_{p,m}$ was peaked at ≈33 nm with

similar FWHMs. Results indicate that the charge state in solution does not interfere the measured electrophoretic mobility of N-GOs by ES-DMA.

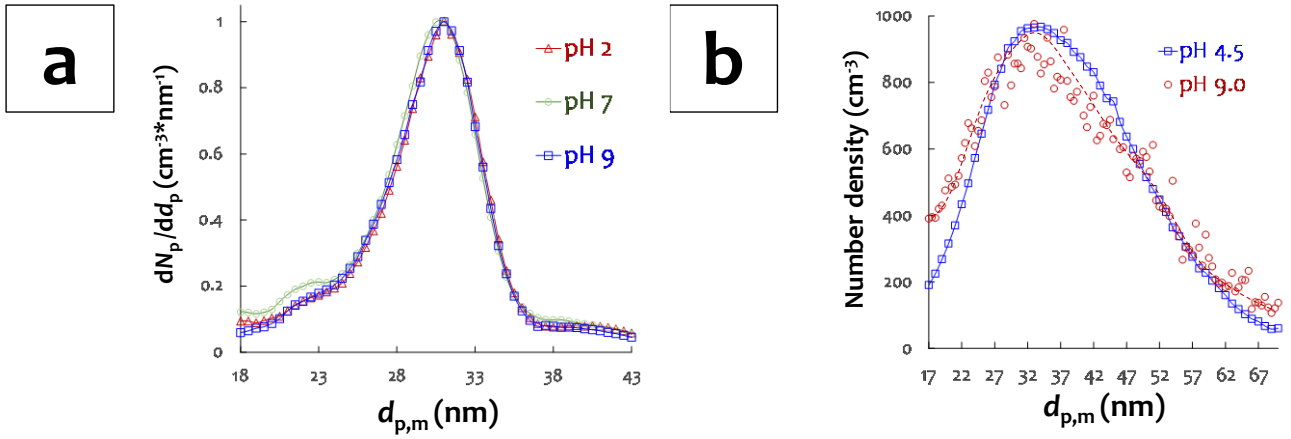

Figure S10. Effect of pH on the measured mobility size distributions. (a) Mobility size distributions of SiO_2 nanoparticles under pH 2, pH 7, and pH 9. (b) Mobility size distributions of N-GO at pH 4.5 and pH 9.0.

8. Derivations of L_t as a Function of $d_{p,m}$

In Sec. 3.3 of the main text, we employ an analytical model to convert $d_{p,m}$ into L_t. The base of assumption used in the model starts from the determination of the drag force of a N-GO, F_D, shown in Eq. S9 based on Stokes' Law: [1]

$$F_D = \frac{3\pi\mu d_{p,m}}{C_c} \qquad \text{(S9)}.$$

F_D is proportional to $d_{p,m}/C_c$. Figure S11 demonstrates the correlations of C_c versus $d_{p,m}$. As seen, C_c is proportional to $d_{p,m}^{-0.9}$ when $d_{p,m}$<100 nm. Hence we use an approximation of $F_D \propto d_{p,m}^{2}$ for the following calculations.

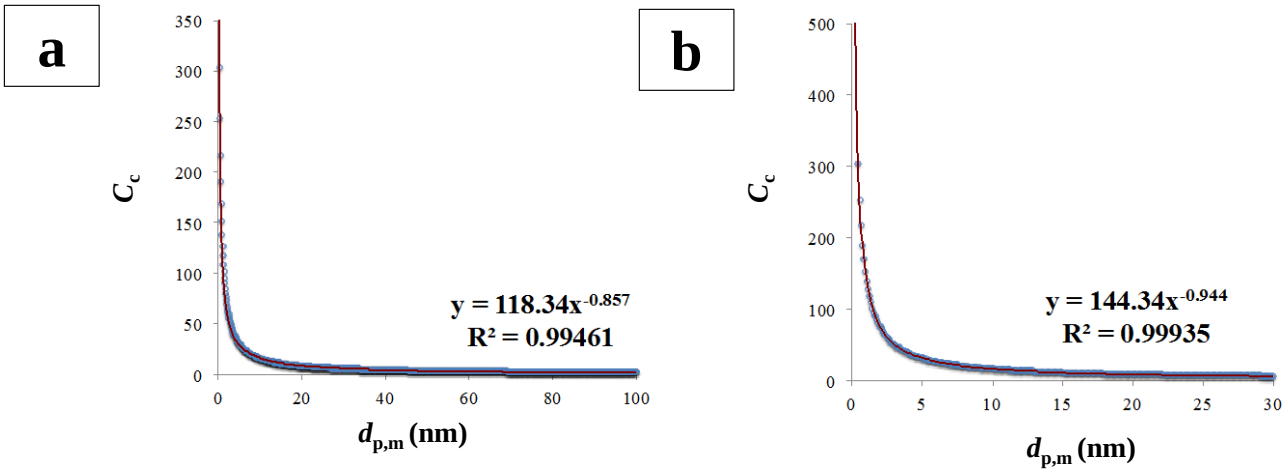

Figure S11. Correlations of C_c versus $d_{p,m.}$ (a) 0.5 nm <$d_{p.m}$< 100 nm. (b) 0.5 nm <$d_{p.m}$< 30 nm.

In DMA measurement, the electrophoretic mobility, Z_e, is determined by a force balance between the electrostatic force, F_e, and the drag force:

$$F_e=Z_{e*}E \qquad \text{(S10)}.$$

Here E is the applied electric field in DMA. Combining Eq. S9 to Eq. S10 we obtain a correlation of $Z_e \propto \frac{1}{d_{p,m}{}^2}$. Knowing the projected area of a N-GO, A_p, is proportional to $d_{p,m}{}^2$, a correlation of Z_e versus A_p is shown in Eq. S11:

$$Z_e=k_1/\, d_{p,m}{}^2= k_2/A_p \qquad \text{(S11)}.$$

Here k_1 and k_2 are fitting constants. For an asymmetric nanoparticle (nanorod, nanotube, or nanocluster), the projected area is an average of its three dimensions[19-21]. Because $L_t >> \delta_{GO}$, A_p is mainly proportional to $L_t{}^2$.

$$A_p=k_3*L_t{}^2 \qquad \text{(S12)}.$$

Where k_3 is a fitting constant. Combining Eq. S11 and Eq. S12, we obtain a correlation of $d_{p,m} = K*L_t$. Here $K=(k_1*k_3/k_2)^{0.5}$.

9. Analysis of N-GOs using Scanning Probe Microscopy (SPM)

A Seiko SPA-400 with a Seiko SPI-3800N probe station was employed at room temperature, tapping mode. A silicon tip was used in dynamic force mode experiments with spring force of 5 N/m and a scan rate of 1 Hz. Figure S12 shows a SPM analysis of a N-GO sample (i.e., without size classification) electrostatically deposited on a mica substrate. We saw a few particles possibly to be N-GO and/or S-NPs, and the height was estimated to be ranging from 0.7 nm to 4.7 nm. As we have described in the main text, identifying these N-GOs via SPM is a significant challenge because of its nanoscale dimensional properties. Note that the lateral size measured by SPM cannot be used for comparison to the results by TEM and ES-DMA due to the limit in resolution.

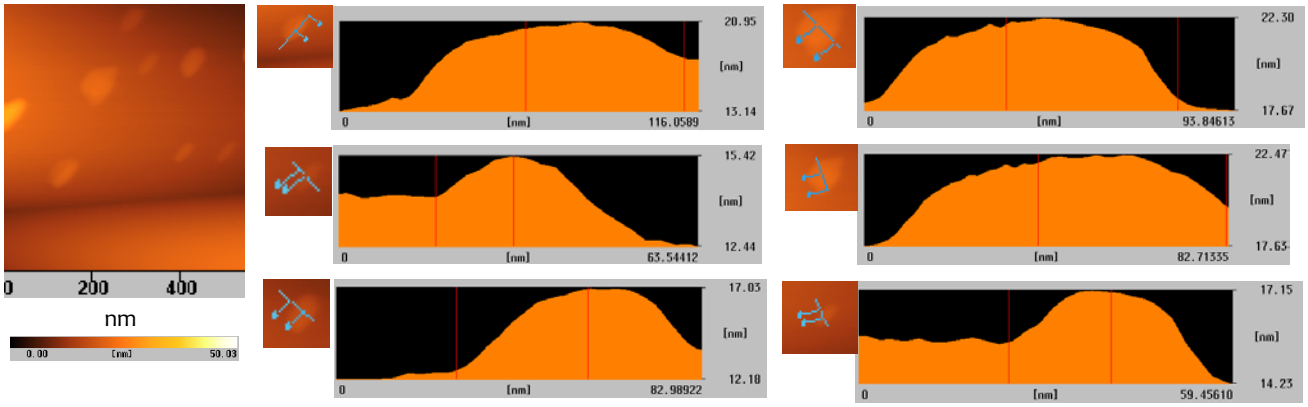

Figure S12. SPM analysis. Left: SPM image of the electrosprayed N-GOs without size classification. Sample was electrostatically deposited on a mica substrate. Right: topographic images.

References

(1) Hinds, W. C. *Aerosol Technology: Properties, Behavior, and Measurement of Airborne Particles*; Second ed.; John Wiley & Sons, 1999.

(2) *Series 3080 Electrostatic Classifiers---Operation and Service Manual*; TSI Inc., 2009.

(3) Tai, J.-T.; Lai, C.-S.; Ho, H.-S.; Yeh, Y.-S.; Wang, H.-F.; Ho, R.-M.; Tsai, D.-H. *Langmuir* **2014**, *30*, 12755.

(4) Tsai, D. H.; Cho, T. J.; DelRio, F. W.; Gorham, J. M.; Zheng, J. W.; Tan, J. J.; Zachariah, M. R.; Hackley, V. A. *Langmuir* **2014**, *30*, 3397.

(5) Tsai, D. H.; DelRio, F. W.; Pettibone, J. M.; Lin, P. A.; Tan, J. J.; Zachariah, M. R.; Hackley, V. A. *Langmuir* **2013**, *29*, 11267.

(6) Tsai, D. H.; Pease, L. F., 3rd; Zangmeister, R. A.; Tarlov, M. J.; Zachariah, M. R. *Langmuir* **2009**, *25*, 140.

(7) Tsai, D. H.; Cho, T. J.; DelRio, F. W.; Taurozzi, J.; Zachariah, M. R.; Hackley, V. A. *J Am Chem Soc* **2011**, *133*, 8884.

(8) Tsai, D. H.; Zangmeister, R. A.; Pease Iii, L. F.; Tarlov, M. J.; Zachariah, M. R. *Langmuir* **2008**, *24*, 8483.

(9) Kaufman, S. L. *Anal Chim Acta* **2000**, *406*, 3.

(10) Pease, L. F.; Elliott, J. T.; Tsai, D. H.; Zachariah, M. R.; Tarlov, M. J. *Biotechnol Bioeng* **2008**, *101*, 1214.

(11) Schniepp, H. C.; Li, J. L.; McAllister, M. J.; Sai, H.; Herrera-Alonso, M.; Adamson, D. H.; Prud'homme, R. K.; Car, R.; Saville, D. A.; Aksay, I. A. *J Phys Chem B* **2006**, *110*, 8535.

(12) Dikin, D. A.; Stankovich, S.; Zimney, E. J.; Piner, R. D.; Dommett, G. H. B.; Evmenenko, G.; Nguyen, S. T.; Ruoff, R. S. *Nature* **2007**, *448*, 457.

(13) Niu, Z. Q.; Chen, J.; Hng, H. H.; Ma, J.; Chen, X. D. *Adv Mater* **2012**, *24*, 4144.

(14) Wang, H. Y.; Wang, G. M.; Ling, Y. C.; Qian, F.; Song, Y.; Lu, X. H.; Chen, S. W.; Tong, Y. X.; Li, Y. *Nanoscale* **2013**, *5*, 10283.

(15) Huang, L.; Li, C.; Shi, G. Q. *J Mater Chem A* **2014**, *2*, 968.

(16) Yang, J. H.; Lin, S. H.; Lee, Y. D. *J Mater Chem* **2012**, *22*, 10805.

(17) Yang, J. H.; Lee, Y. D. *J Mater Chem* **2012**, *22*, 8512.

(18) *Reports of Investigation: SRM8011, SRM8012, SRM8013*, National Institute of Standards and Technology, United States of America.

(19) Song, D. K.; Lenggoro, I. W.; Hayashi, Y.; Okuyama, K.; Kim, S. S. *Langmuir* **2005**, *21*, 10375.

(20) Pease, L. F.; Tsai, D. H.; Fagan, J. A.; Bauer, B. J.; Zangmeister, R. A.; Tarlov, M. J.; Zachariah, M. R. *Small* **2009**, *5*, 2894.

(21) Pease, L. F.; Tsai, D. H.; Brorson, K. A.; Guha, S.; Zachariah, M. R.; Tarlov, M. J. *Anal Chem* **2011**, *83*, 1753.